

Supplementary Information

Crystal-amorphous NiO/MoO₂ with high-density interface for hydrogen evolution

Ya-Nan Zhou ^a, Meng-Xuan Li ^a, Zhuo-Ning Shi ^a, Jian-Cheng Zhou ^a, Bin Dong ^{*a},

Wenchun Jiang ^b, Bin Liu ^a, Jian-Feng Yu ^a, Yong-Ming Chai ^{*a}

a State Key Laboratory of Heavy Oil Processing, College of Chemistry and Chemical Engineering,

China University of Petroleum (East China), Qingdao 266580, PR China

b College of New Energy, China University of Petroleum (East China), Qingdao, 266580, PR China

* Corresponding author. Email: dongbin@upc.edu.cn (B. Dong); ymchai@upc.edu.cn (Y.M. Chai)

Tel: +86-532-86981156, Fax: +86-532-86981156

Table of content

Experimental section	3
<i>Characterization</i>	3
<i>Electrochemical measurements</i>	3
<i>DFT calculation</i>	4
Structure and morphology study	5
<i>Morphology characterization</i>	6
<i>XRD results</i>	8
<i>HRTEM results</i>	9
<i>Surface elements</i>	10
HER performance measurements	12
<i>HER activity</i>	12
<i>Morphologies after HER</i>	15
DFT calculations	23
References	24

Characterization

SEM performed on a JEM 2100F microscope and TEM acquired using FEI Tecnai G20 at 200 kV were taken to detect the morphology and lattice information of synthesized samples. The crystal structure of the samples is characterized by X-ray diffraction (XRD) with Cu K α radiation ($\lambda = 1.54 \text{ \AA}$) on the Brook D8 advance equipment. Energy dispersive X-ray spectroscopy (EDX) is recorded on the Hitachi S-4800 to obtain the element composition and distribution of the resulting sample. X-ray photoelectron spectroscopy (XPS) data is collected with Thermo Fisher K-alpha 250Xi to study the surface chemical and valence information of materials.

Electrochemical measurements

Electrochemical performance measurements were performed at room temperature by a standard three-electrode system with GAMRY Reference 3000 electrochemical equipment. The cut MoNi foam (1 cm \times 2 cm) was ultrasonically treated with hydrochloric acid, acetone, ethanol and deionized water, respectively, for 30 min to remove the surface impurity. All electrochemical measurements were conducted under the same conditions in 1.0 M KOH. The obtained samples, graphite rod electrode and saturated calomel electrode were used as working electrode, counter electrode and reference electrode, respectively. The scan rate of linear sweep voltammetry curves was maintained at 5 mV s $^{-1}$. All the electrode potential were converted to reversible hydrogen electrode (RHE) via the Nernst equation: $E_{\text{RHE}} = E_{\text{SCE}} + 0.0592 \text{ pH} + E^0_{\text{SCE}}$ ($E^0_{\text{SCE}} = 0.245 \text{ V}$). All the polarization curves were iR corrected. The CV curves with different scanning rates are employed to determine the double-layer capacitances (C_{dl}). The stability of sample was evaluated via both chronopotentiometry and fast CV cycles with a rate of 40 mV s $^{-1}$ for 4000 sweeps. The frequency of electrochemical impedance spectroscopy (EIS) was range from 10 5 Hz to 0.1 Hz with AC voltage of 5 mV. All the overpotential in this work is converted

to RHE unless indicated.

DFT calculation

The density functional theory (DFT) calculations were carried out by using the material studio. The exchange-correlation interaction was described by generalized gradient approximation (GGA) with the Perdew-Burke-Ernzerhof (PBE) functional.¹⁻³ The energy cutoff was set to 490 eV. The Monkhorst-Pack k-point mesh was set as $3 \times 3 \times 5$, $1 \times 3 \times 1$ and 2×2 for NiO (110), MoO₂ (200), and NiO/MoO₂ (101) surface models, respectively. The convergence criterion in geometry optimization was set as 10^{-5} eV/atom for energy. For the construction of surface models, a vacuum of 20 Å was used to eliminate interactions between periodic structures.

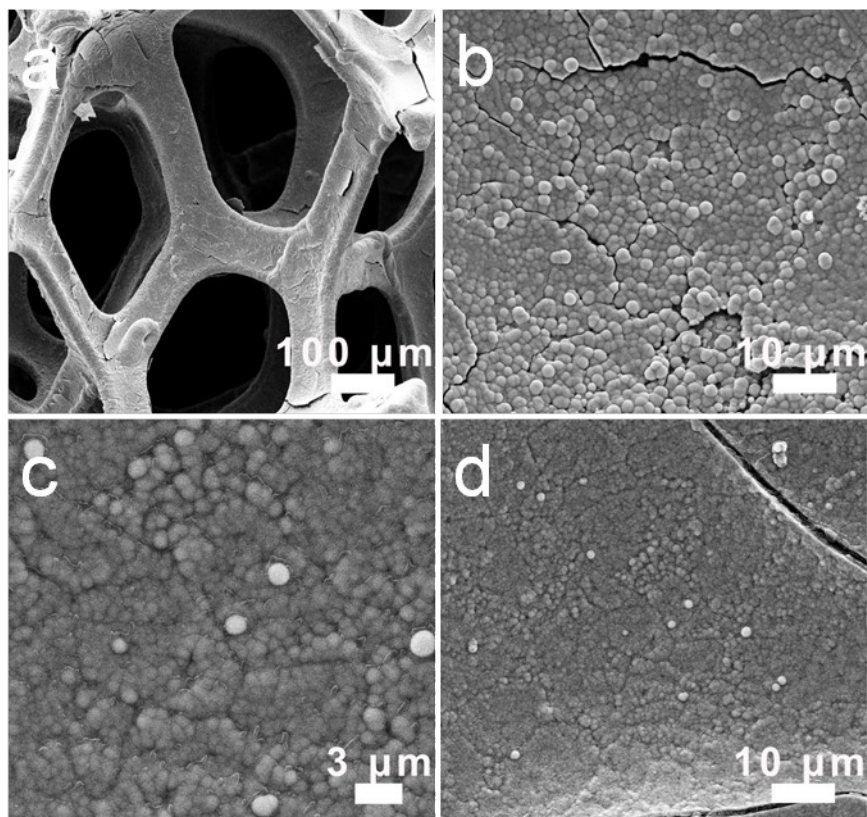


Fig. S1. SEM morphologies of (a and b) commercial MoNi foam, (c and d) NiO/MoO₂-100 sample.

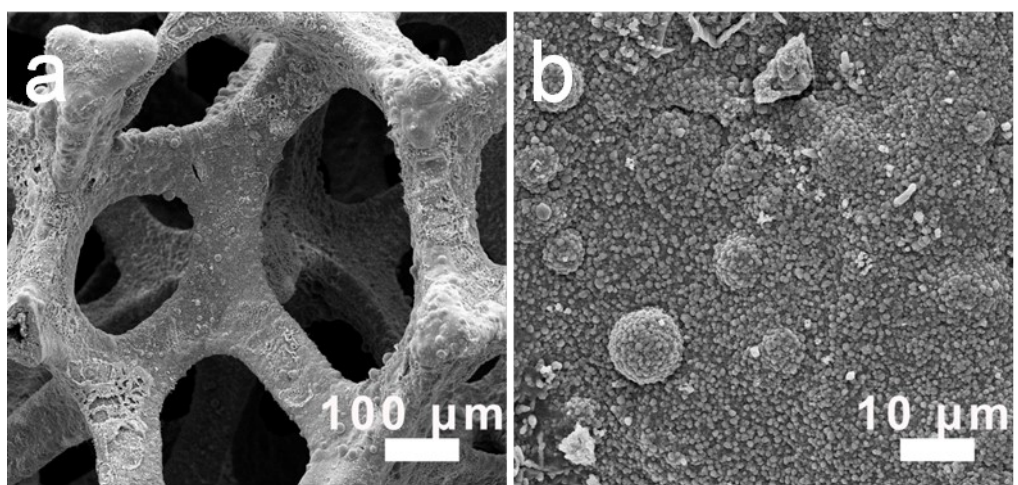


Fig. S2. SEM morphologies of NiO/MoO₂-100-2.

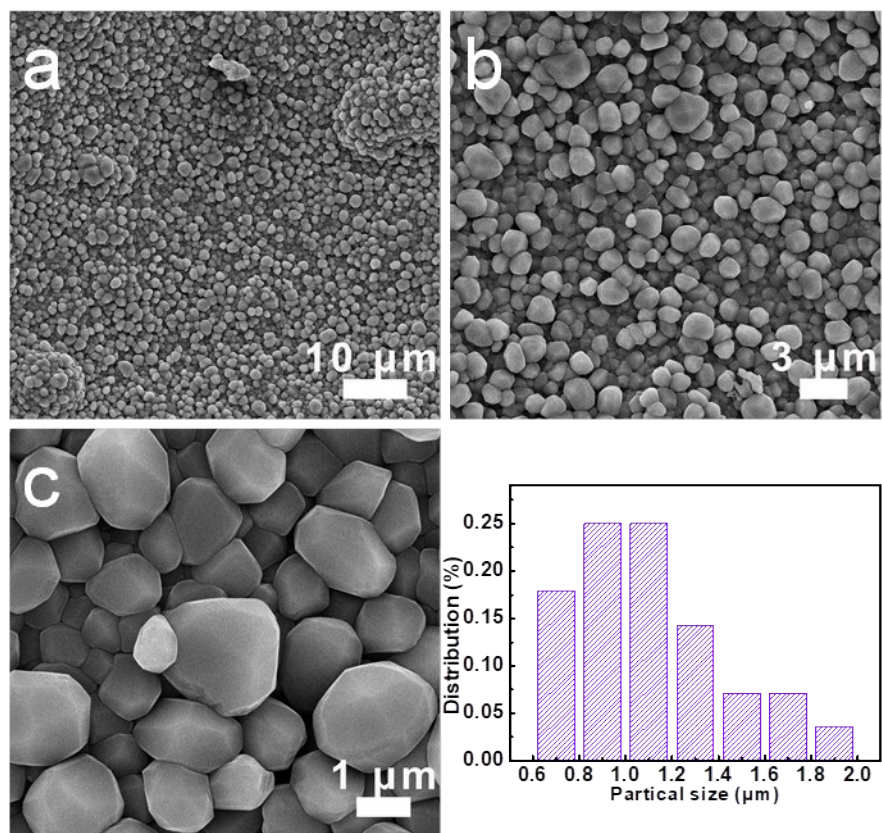


Fig. S3. Morphologies of Ni/Mo-2 and corresponding particle distribution.

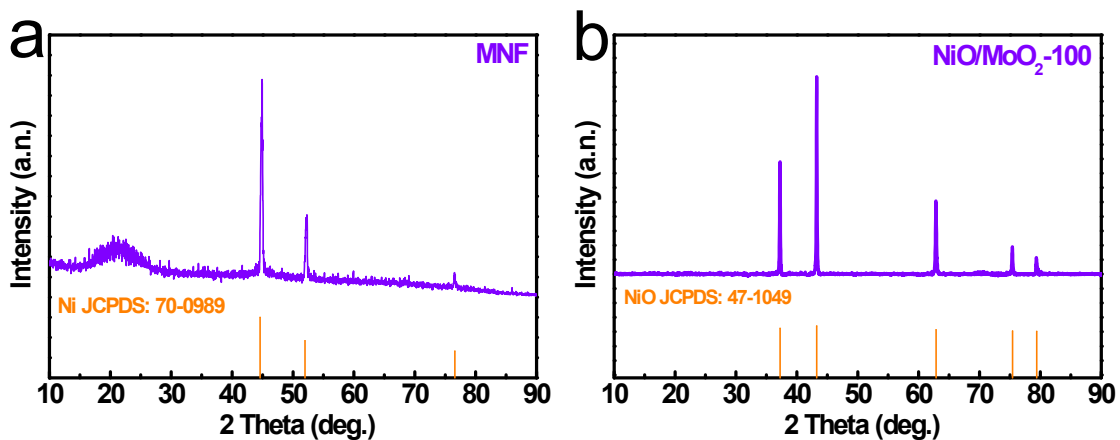


Fig. S4. XRD pattern of (a) MNF and (b) NiO/MoO₂-100.

1
2
3

1
2
3

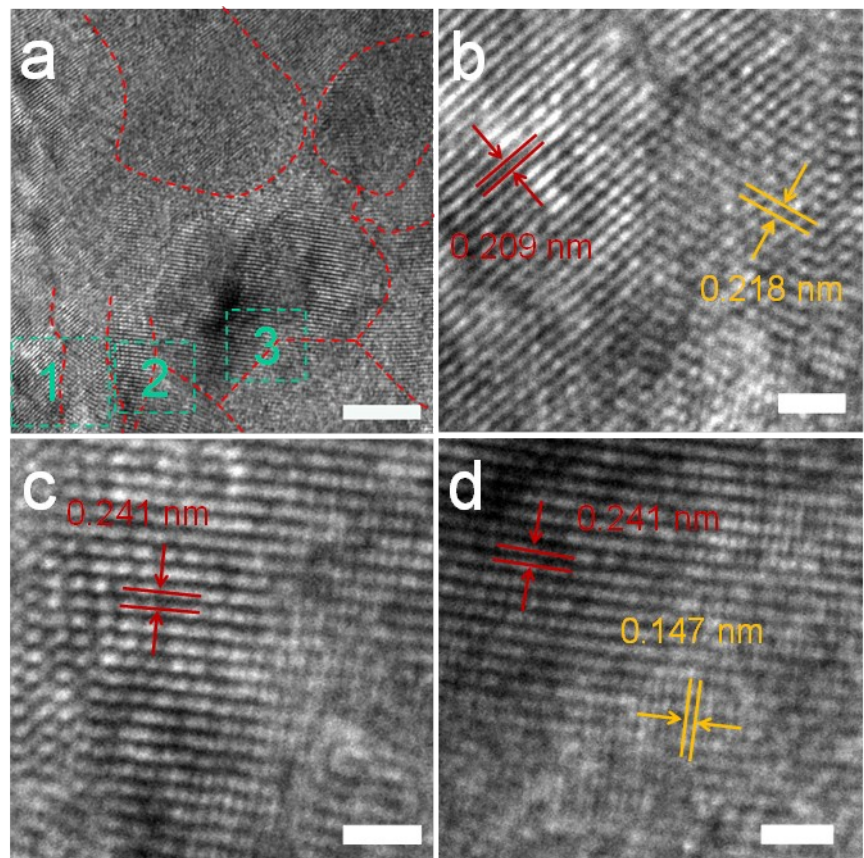


Fig. S5. HRTEM of NiO/MoO₂-100-2. (b), (c), (d) are the region of 1, 2, 3, respectively.

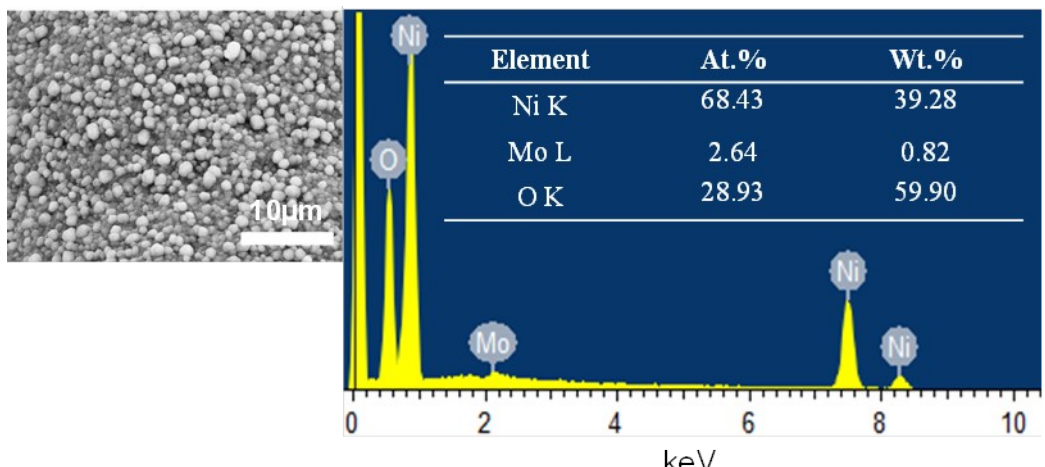
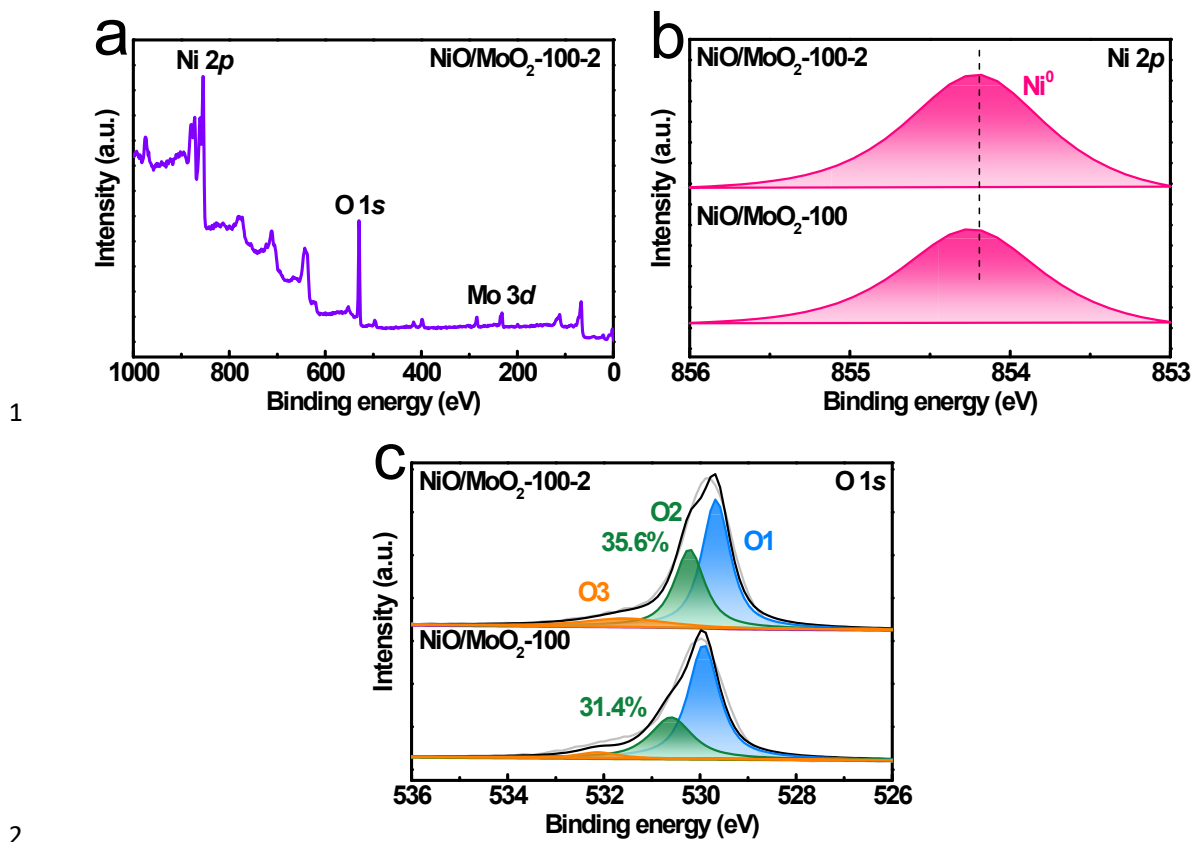


Fig. S6. EDX spectrum and element contents of Mo, Ni, O in NiO/MoO₂-100-2.

1
2
3



2 Fig. S7. (a) XPS survey scan of NiO/MoO₂-100-2. High-resolution XPS of (b) Ni 2p and (c)
3 O 1s of NiO/MoO₂-100-2.

4

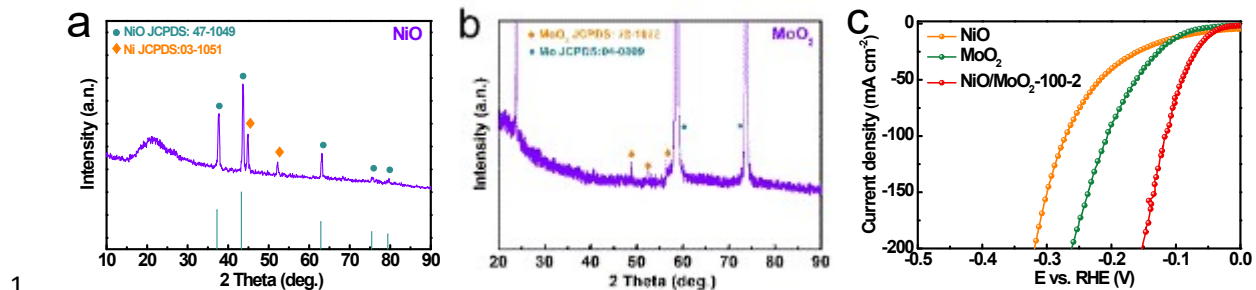


Fig. S8. XRD pattern of (a) NiO and (b) MoO₂ and (c) corresponding HER activity.

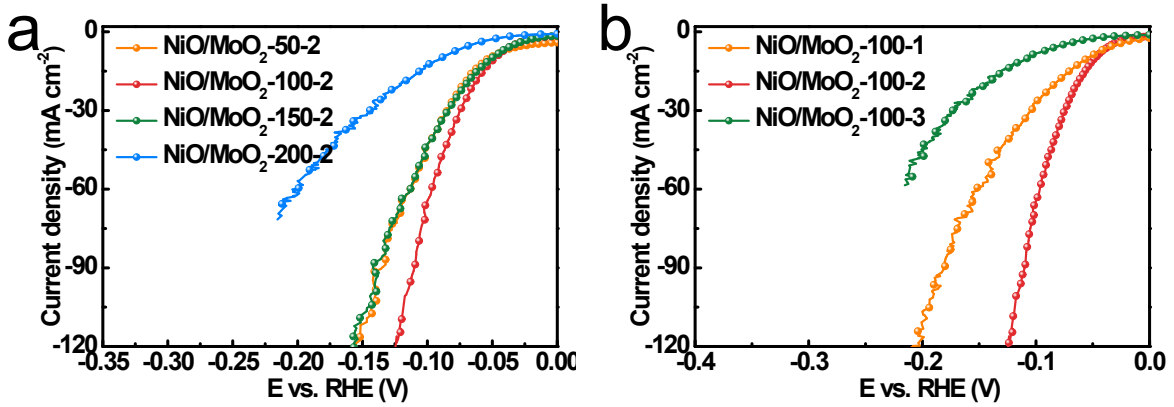
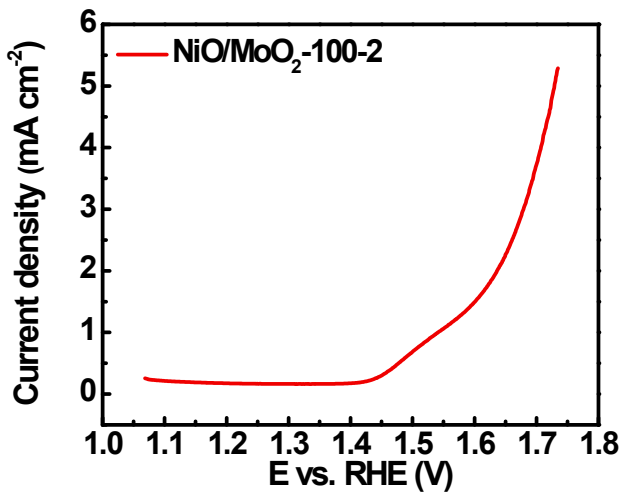
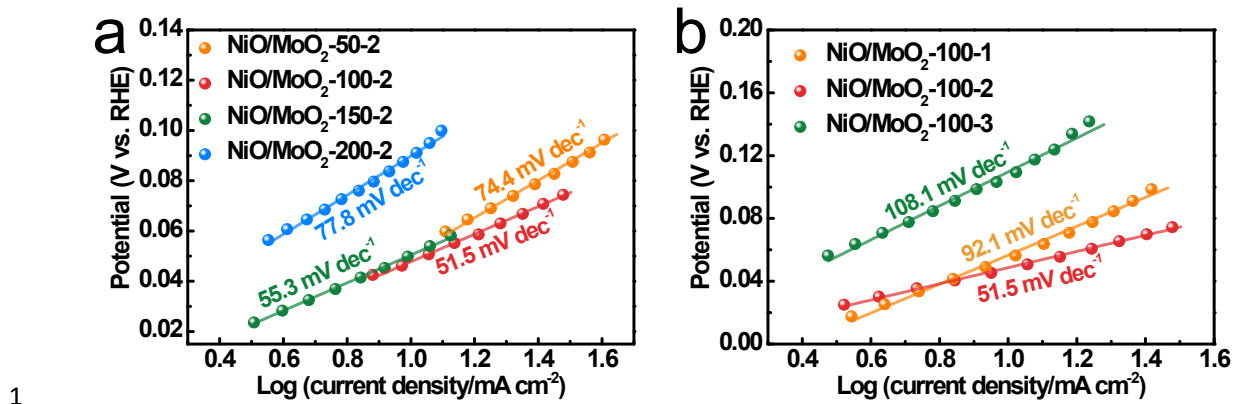


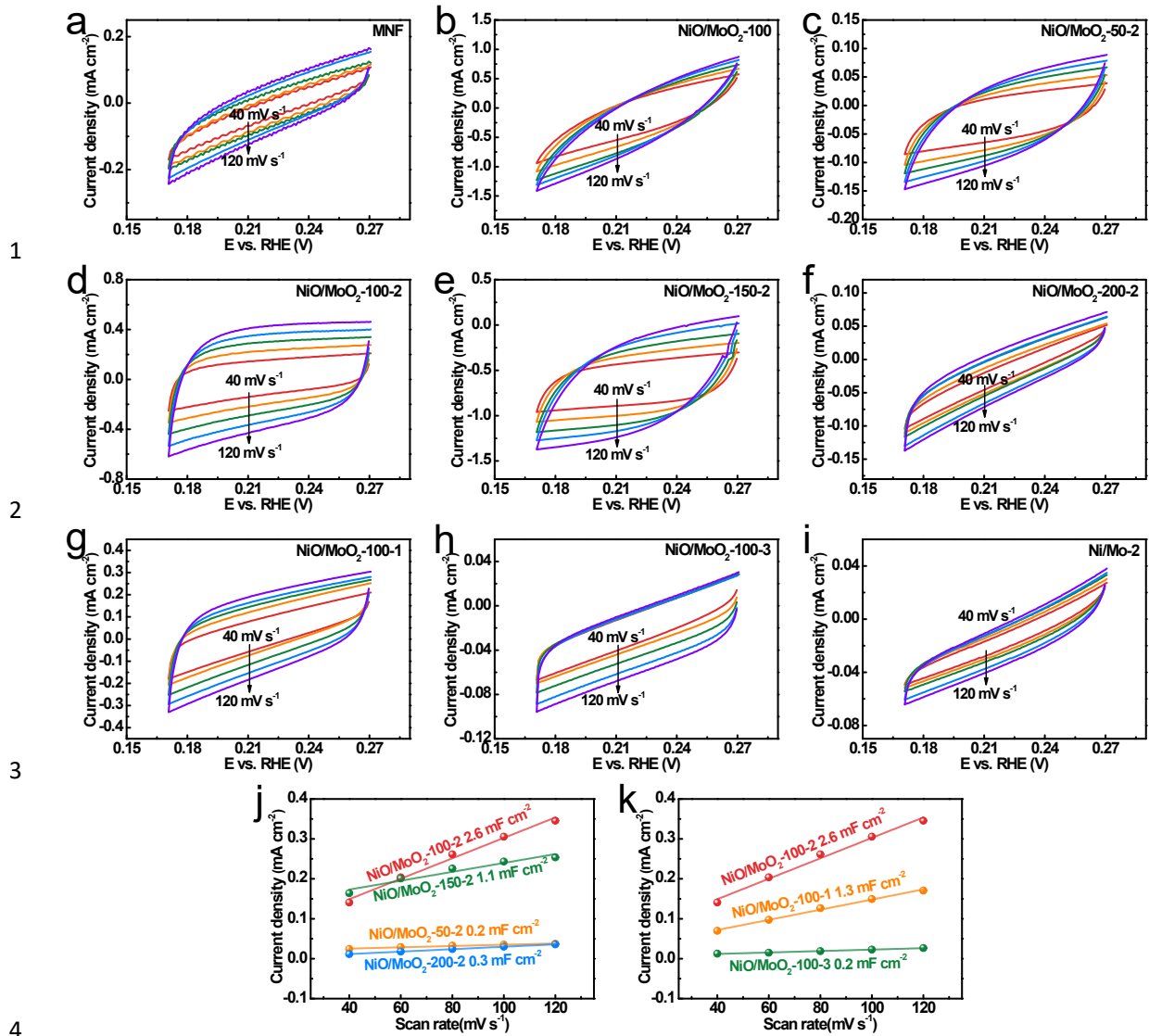
Fig. S9. Polarization curves of NiO/MoO_2 -*s-h* at (a) different oxidation time (*s*) and (b) molten-salt treatment time (*h*).

1

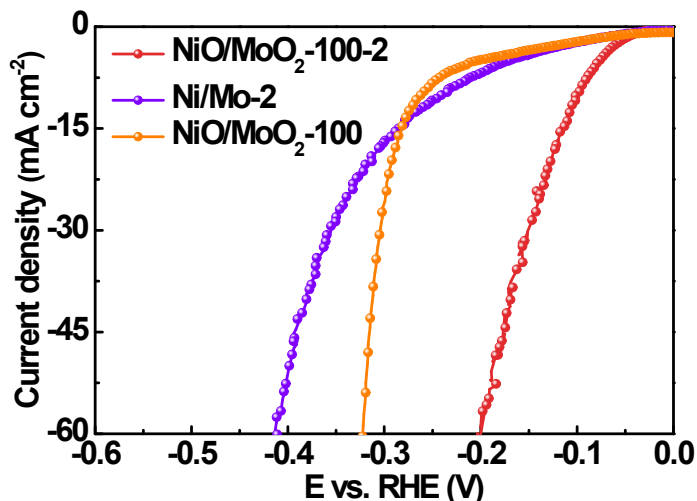
2 **Fig. S10.** Linear sweep voltammetry plot for water oxidation of NiO/MoO₂-100-2.







5 **Fig. S12.** (a-i) CV curves of all obtained samples with scan rate from 40 to 120 mV s⁻¹ within
6 the potential window of 0.17-0.27 V vs. RHE (clockwise) and (j and k) corresponding C_{dl}
7 values.

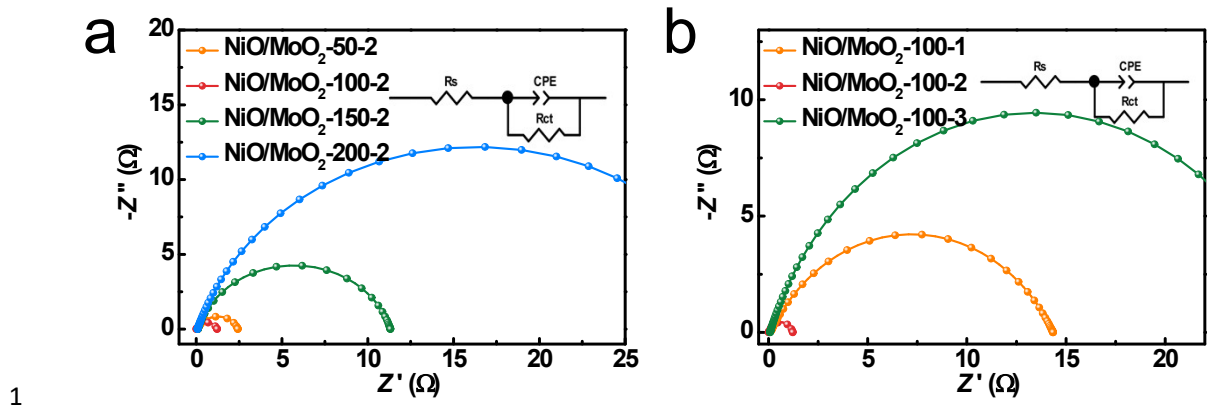


1

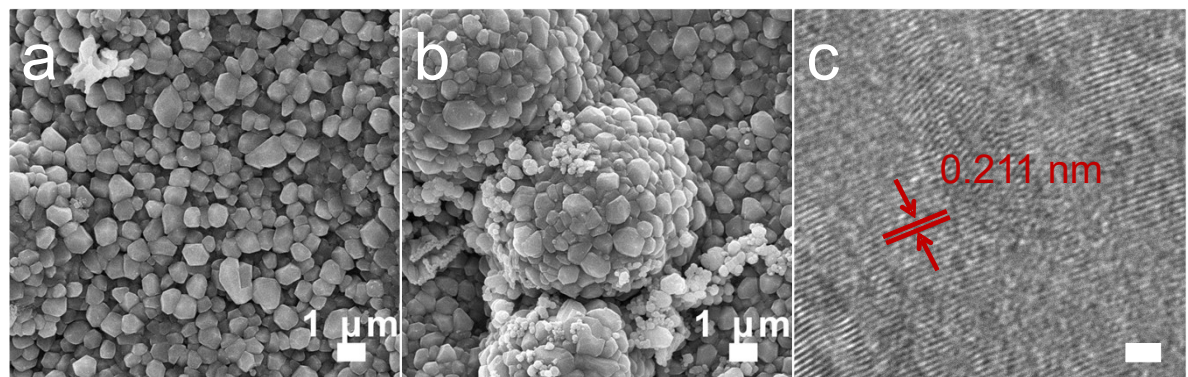
Fig. S13. Linear sweep voltammetry curves polarization curves of Ni/Mo-2, NiO/MoO₂-100, NiO/MoO₂-100-2 after normalized by the electrochemical active surface area.

4 Electrochemical active surface area = C_{dl}/C_s

5 Where, is the specific capacitance of planar surface with atomically smooth under identical
 6 electrolyte condition. We use general value of $40 \mu\text{F cm}^{-2}$.



2 **Fig. S14.** EIS of NiO/MoO₂-*s-h* at (a) different oxidation time (*s*) and (b) molten-salt
3 treatment time (*h*).



1 **Fig. S15.** Morphologies of NiO/MoO₂-100-2 (a) before and (b and c) after long-term HER
2 test. Scale bar: 1 nm.
3

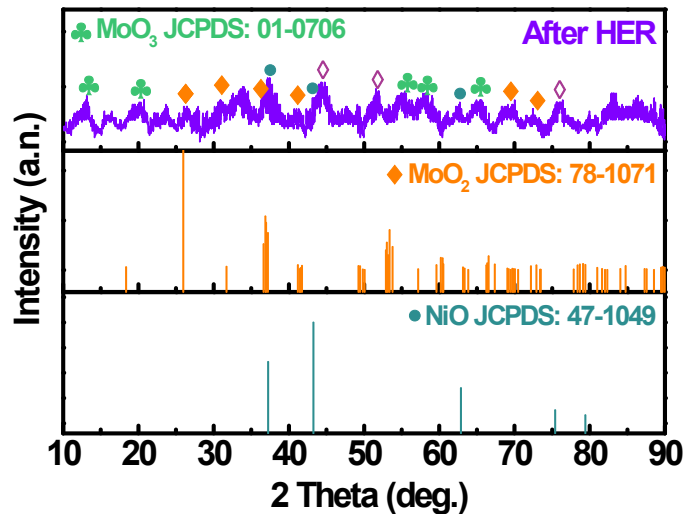
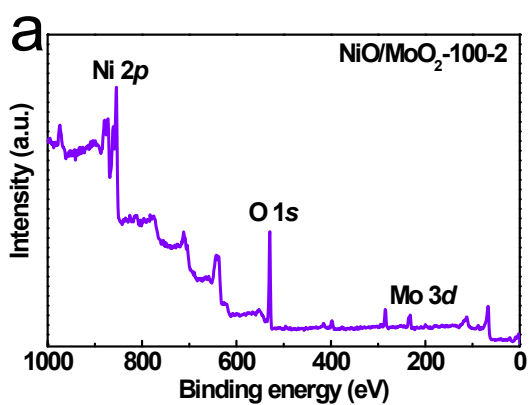
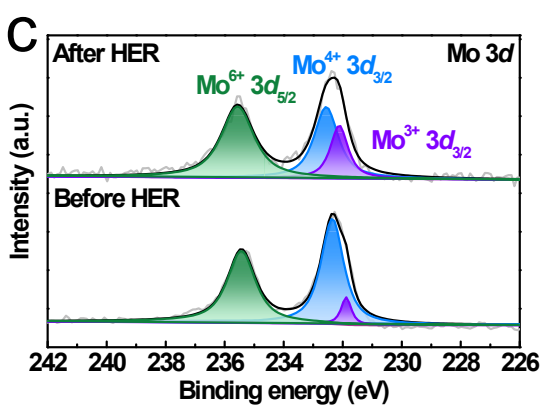


Fig. S16. XRD pattern of NiO/MoO₂-100-2 after 40 h HER test.

1



2



3

Fig. S17. (a) XPS survey scan, and high-resolution (b) Ni 2p, (c) Mo 3d, (d) O 1s spectra of NiO/MoO₂-100-2 after 40 h HER test.

4

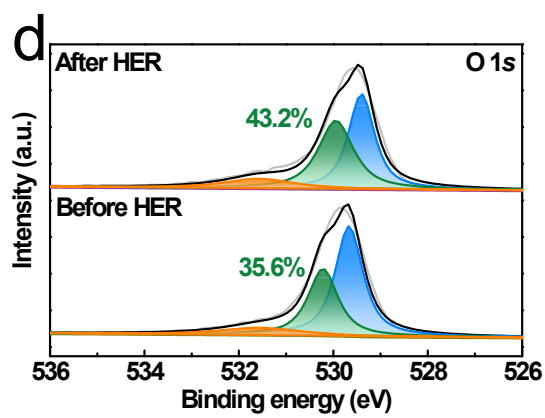
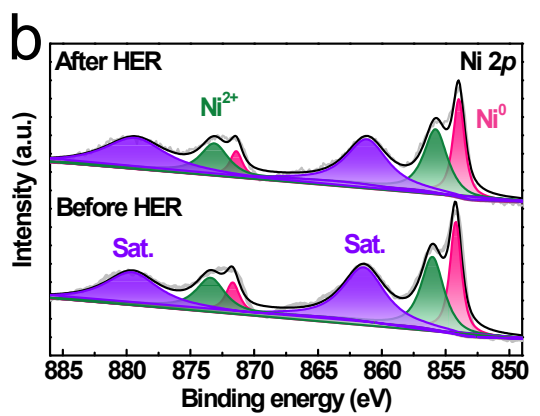


Table S1. Comparison of the HER activity of NiO/MoO₂-100-2 with the other NiO-based OER electrocatalysts in 1.0 M KOH.

Electrocatalyst	j (mA cm ⁻²)	η (mV)	b (mV dec ⁻¹)	Ref.
NiO/MoO₂-100-2	10	48	51.5	This work
NiO_x@BCNTs	10	79	122	[4]
Ni-BDT-A	10	80	70	[5]
Ni/NiO	10	180	135	[6]
NiO NRs-m-Ov	10	110	100	[7]
Ni/NiO/NCW	10	105.3	55.2	[8]
Ni/NiO-3.8	10	90	41	[9]
Ni/NiO CNTs	10	98	67	[10]
MoS_x@NiO	10	406	43	[11]
Ni/NiO-0.5C	10	161	99	[12]
NiO-300	10	424	105	[13]
Fe_{11%}-NiO/NF	10	88	49.7	[14]
Ni/NiO@HGP_xO_y	10	205	80	[15]
Ni/NiO	10	41	59	[16]

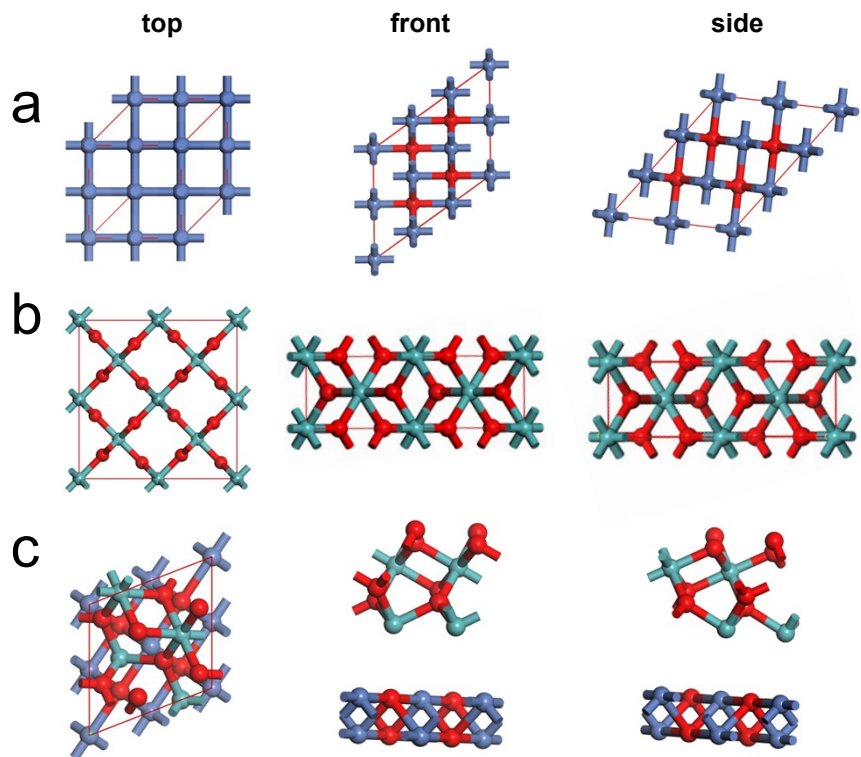


Fig. S18. Different views of (a) NiO, (b) MoO₃ and (c) NiO/MoO₃ simulated models.

Reference

- 1 J.P. Perdew, M. Ernzerhof and K. Burke, Rationale for Mixing Exact Exchange with Density Functional Approximations, *J. Chem. Phys.*, 1996, **105**, 9982–9985.
- 2 G. Kresse and D. Joubert, From ultrasoft pseudopotentials to the projector augmented-wave method, *Phys. Rev. B*, 1999, **59**, 1758–1775.
- 3 J.P. Perdew, K. Burke and M. Ernzerhof, Generalized gradient approximation made simple, *Phys. Rev. Lett.*, 1996, **77**, 3865–3868.
- 4 J. Wang, S. Mao, Z. Li, Z. Wei, H. Wang, Y. Chen and Y. Wan, Dominating role of NiO on the interface of Ni/NiO for enhanced hydrogen evolution reaction, *ACS Appl. Mater. Interfaces*, 2017, **9**, 7139–7147.
- 5 C.Y. Hu, Q.Y. Ma, S.-F. Hung, Z.-N. Chen, D.H. Ou, B. Ren, H.M. Chen, G. Fu and N.F. Zheng, In situ electrochemical production of ultrathin nickel nanosheets for hydrogen evolution electrocatalysis, *Chem*, 2017, **3**, 122–133.
- 6 A.Y. Faid, A.O. Barnett, F. Seland and S. Sunde, Ni/NiO nanosheets for alkaline hydrogen evolution reaction: In situ electrochemical-Raman study, *Electrochim. Acta*, 2020, **361**, 137040.
- 7 T. Zhang, M.-Y. Wu, D.-Y. Yan, J. Mao, H. Liu, W.-B. Hu, X.-W. Du, T. Ling and S.-Z. Qiao, Engineering oxygen vacancy on NiO nanorod arrays for alkaline hydrogen evolution, *Nano Energy*, 2018, **43**, 103–109.
- 8 H. Han, S. Park, D. Jang and W.B. Kim, N-doped carbon nanoweb-supported Ni/NiO heterostructure as hybrid catalysts for hydrogen evolution reaction in an alkaline phase, *J. Alloys Compd.*, 2021, **853**, 157338.

- 9 L. Zhao, Y. Zhang, Z.L. Zhao, Q.-H. Zhang, L.-B. Huang, L. Gu, G. Lu, J.-S. Hu and L.-J. Wan, Steering elementary steps towards efficient alkaline hydrogen evolution via size-dependent Ni/NiO nanoscale heterosurfaces, *Natl. Sci. Rev.*, 2020, **7**, 27–36.
- 10 L.J. Yang, X.C. Zhao, R.Z. Yang, P.X. Zhao, Y.T. Li, P. Yang, J.C. Wang and D. Astruc, In-situ growth of carbon nanotubes on Ni/NiO nanofibers as efficient hydrogen evolution reaction catalysts in alkaline media, *Appl. Surf. Sci.*, 2019, **491**, 294–300.
- 11 Z.H. Ibupoto, A. Tahira, P.Y. Tang, X.J. Liu, J.R. Morante, M. Fahlman, J. Arbiol, M. Vagin and A. Vomiero, MoS_x@NiO Composite Nanostructures: An Advanced Nonprecious Catalyst for Hydrogen Evolution Reaction in Alkaline Media, *Adv. Funct. Mater.*, 2019, **29**, 1807562.
- 12 P. Wang, X. Zhang, Y. Wei and P. Yang, Ni/NiO nanoparticles embedded inporous graphite nanofibers towards enhanced electrocatalytic performance, *Int. J. Hydrogen Energy*, 2019, **44**, 19792–19804.
- 13 A. Mondal, A. Paul, D.N. Srivastava and A.B. Panda, NiO hollow microspheres as efficient bifunctional electrocatalysts for Overall Water-Splitting, *Int. J. Hydrogen Energy*, 2018, **43**, 21665–21674.
- 14 Z.C. Wu, Z.X. Zou, J.S. Huang and F. Gao, Fe-doped NiO mesoporous nanosheets array for highly efficient overall water splitting, *J. Catal.* 2018, **358**, 243–252.
- 15 J. Wang, Y.N. Xie, Y.Y. Yao, X. Huang, M. Willinger and L.D. Shao, Ni/NiO nanoparticles on a phosphorous oxide/graphene hybrid for efficient electrocatalytic water splitting, *J. Mater. Chem. A*, 2017, **5**, 14758–14762.
- 16 Y. Jiao, W.Z. Hong, P.Y. Li, L.X. Wang and G. Chen, Metal-organic framework derived Ni/NiO micro-particles with subtle lattice distortions for high-performance electrocatalyst and

supercapacitor, *Appl. Catal. B Environ.*, 2019, **244**, 732–739.